====== CONDENSED ======
====== MATTER ======

Transition to a Magnon Bose−Einstein Condensate

P. E. Petrov[a,b], G. A. Knyazev[a,b], A. N. Kuzmichev[a], P. M. Vetoshko[a,c,d],
V. I. Belotelov[a,b,c], and Yu. M. Bunkov[a,*]

[a] Russian Quantum Center, Skolkovo, Moscow, 121205 Russia
[b] Moscow State University, Moscow, 119992 Russia
[c] Vernadsky Crimean Federal University, Simferopol, 295007 Russia
[d] Kotelnikov Institute of Radio Engineering and Electronics, Russian Academy of Sciences, Moscow, 125009 Russia
***e-mail: y.bunkov@rqc.ru**
Received November 16, 2023; revised November 30, 2023; accepted November 30, 2023

Parameters of the transition from classical dynamics of spin waves to the formation of a coherent magnon Bose−Einstein condensate have been obtained experimentally for the first time. The studies are performed on an yttrium iron garnet film beyond the radio frequency excitation region; thus, the coherent state of magnons is an eigenstate rather than a state induced by an external radio frequency field. The critical magnon density at the formation of the Bose−Einstein condensate is in good agreement with a theoretically predicted value. The transition is obtained at room temperature, which is possible owing to a small mass of magnons and their high density.

The formation of the coherent quantum state of matter, which is a new aggregate state, is mainly determined by Bose−Einstein condensation. This state manifests itself in quantum phenomena such as superconductivity of electrons and superfluidity of atoms. Bose−Einstein condensation was directly observed in a rarefied gas of atoms [1, 2] and photons [3−5]. In addition to particles themselves, quasiparticles such as magnons [6], phonons [7], rotons [8], excitons [9], polaritons [10], and coupled exciton−polariton states [11] can also form macroscopic quantum states. Under conditions of Bose−Einstein condensation, a macroscopic number of quasiparticles are in a single quantum state. It arises if a sufficient number of nonequilibrium quasiparticles are excited, and its characteristics are determined by the well-known Bose−Einstein condensation formula

$$T_{\mathrm{BEC}} = \kappa_0 \frac{\hbar^2}{k_\mathrm{B} m}\left(\frac{N}{V_\mathrm{s}}\right)^{2/3}, \quad \kappa_0 = \frac{2\pi}{\left[\zeta\left(\frac{3}{2}\right)\right]^{2/3}} \simeq 3.31, \ (1)$$

where T_{BEC} is the critical temperature of Bose−Einstein condensation; m and N/V_s are the mass and number density of quasiparticles, respectively; $\hbar$ is the reduced Planck constant; k_B is the Boltzmann constant; and ζ is the Riemann zeta function.

The formation of the Bose−Einstein condensate (BEC) of magnons (mBEC), which are excitation quasiparticles in a magnetically ordered system, was first discovered in 1984 in antiferromagnetic super-

fluid ^{3}He-B [6, 12−14]. It was revealed by the spontaneous restoration of the coherence of magnons after their pulsed excitation and initial dephasing in an inhomogeneous magnetic field [15, 16]. A specific feature of the formation of the magnon coherent state in ^{3}He-B is a peculiar mechanism of spatial redistribution of spins due to the superfluid counterflow of superfluid components with opposite magnetization. Specifically this mechanism led to the formation of a domain with uniform precession [17, 18].

However, this mechanism is absent in most other cases of the formation of the Bose−Einstein condensate when condition (1) is satisfied (in particular, the mBEC in solids under consideration). In this case, the coherent state of magnons is provided by their interaction with each other. In this paper, we consider the formation of the BEC of stationary magnons with $k = 0$, which is similar in many respects to the formation of an atomic BEC. Under some experimental conditions, propagating magnons with nonzero k have a lower energy than magnons at rest. Here, coherent effects are also observed [19] but they are beyond the scope of this study because of the specificity of this case.

The magnon BEC at $k = 0$ was found in systems with coupled nuclear−electron precession in some antiferromagnets [20−22]. In particular, the suppression of spin−spin relaxation T^2 during the formation of the magnon Bose−Einstein condensate was found in these systems. It was revealed that the duration of the induction signal from the magnon BEC is an order

of magnitude longer than that expected from the T^2 value obtained by the spin-echo method. This effect also explains the results presented in this paper below.

A real breakthrough was achieved with the discovery of the mBEC in yttrium iron garnet (YIG) films at room temperature [23, 24]. Magnons in YIG films magnetized perpendicular to the sample plane have the minimum energy at zero wave vector k and are characterized by repulsive interactions, as in ^{3}He-B. Therefore, the mBEC is formed by steady-state magnons, as in the atomic BEC. Further on, we refer to it as the atomic-type mBEC.

Since magnons are quasiparticles in magnetically ordered systems, their equilibrium density is determined by the temperature of the system. Note that this density is always lower than the magnon density required for Bose–Einstein condensation. However, the magnon density can be increased significantly by the excitation of nonequilibrium magnons. The critical magnon density for magnon Bose–Einstein condensation in different systems can be calculated from the parameters of the magnon spectrum. For example, for the system under consideration (the YIG film magnetized perpendicular to the surface), the critical magnon density corresponds to the dynamic deviation of the magnetization by an angle of 2.5° [25].

In a system of nonequilibrium magnons, a change in the projection $\mathcal{S}_z$ of the total spin on the direction of the external magnetic field plays the role of the particle density $\mathcal{N}$. The excitation of nonequilibrium magnons leads to a decrease in the longitudinal magnetization $\mathcal{S}_z$ of the system by a value proportional to $1 - \cos\beta$, where β is the angle of dynamic deviation of the equilibrium magnetization [26, 27]. The interaction between magnons shifts the precession frequency away from the Larmor frequency by $\Delta\omega$, which determines the coherence length and the critical velocity of the superfluid magnon flow [26, 27].

A significant advantage of magnon superfluidity is that the superfluid state with the deviated and precessing magnetization is the ground state of the system at a given magnon density. Therefore, it can be steadily kept by replacing the evaporating magnons using external pump. Note that new excited magnons are created in the state of the existing Bose–Einstein condensate [28]. Moreover, the pump radio frequency determines the chemical potential and the corresponding density of nonequilibrium magnons [6, 29]. As a result, the magnon density is determined by the difference between the Larmor frequency and the pump radio frequency and independent of the radio-frequency field amplitude, which directly contradicts the intuitive approach of some researchers [30, 31]. The magnon density in the condensate can be changed by varying the frequency (or magnetic field) at a fixed radio frequency pump [32].

The distribution and dynamics of magnons in YIG films are generally investigated using the effect of Brillouin scattering. It is widely applied to study the Bose–Einstein condensation of magnons in in-plane magnetized films [19, 33]. In this case, parametrically excited spin waves are concentrated at the minimum energy corresponding to magnons with nonzero wave vector k. Note also that the magnon Bose–Einstein condensation was also found in this geometry for magnons at $k = 0$ at resonant excitation [34].

However, the method of Brillouin scattering is not applicable to study magnons with zero k. An optical setup developed at the Russian Quantum Center makes it possible to investigate the spatial distribution of the density and phase of the magnetization precession for magnons with zero k. This setup uses the Faraday rotation of the polarization of light interacting with the transverse component of the precessing magnetization. This setup was designed to study the processes of magnon Bose–Einstein condensation in perpendicularly magnetized YIG films. The setup and its characteristics were described in detail in [35, 36].

Using this setup, we thoroughly studied the spatial distribution of the precessing magnetization at weak and strong excitations of magnons as a function of the external magnetic field [37]. Two modes of the magnon distribution were experimentally obtained: the spin wave mode and the coherent precession mode corresponding to magnon Bose–Einstein condensation. The experiments were carried out on a 6-μm-thick YIG film in the form of a 4.5 × 1.5 mm ellipse magnetized perpendicular to the plane. The magnetic resonance was excited using a strip line 0.2 mm wide oriented perpendicular to the major axis of the sample. It was demonstrated that the precessing magnetization at a relatively low pump power deviates significantly only in the excitation region corresponding to the position of the strip line. Spin waves transmitting the excitation beyond this region were also observed.

The distribution of the precessing magnetization changed radically with an increase in the pump power to 6 mW. In a wide range of fields, we obtained the spatially uniform amplitude and phase of the precession throughout the sample, except for the excitation region where the signal is characterized by a larger amplitude and a deviated phase. This state can be identified as the magnon Bose–Einstein condensate.

We also performed a computer simulation of the experimental conditions using the MuMax^3 micromagnetic simulation package [38], which yielded a close fit to the experimental results at a pump power of 0.05 mW, when spin waves propagating from the excitation region are formed. However, within the semiclassical calculation based on the Landau–Lifshitz–Gilbert equations, we could not obtain the coherent precession state beyond the excitation region under varying both the pump power and the physical parameters of the YIG film in wide ranges [37]. Thus, we
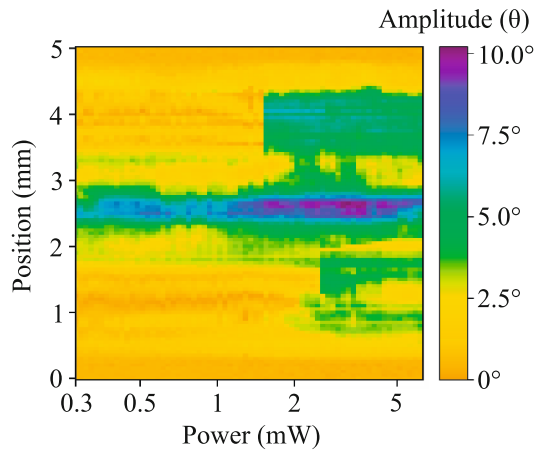
Fig. 1. (Color online) Amplitude distribution of the magnetization precession signal over the sample under varying the pump power in the excitation strip located in the middle of the sample.
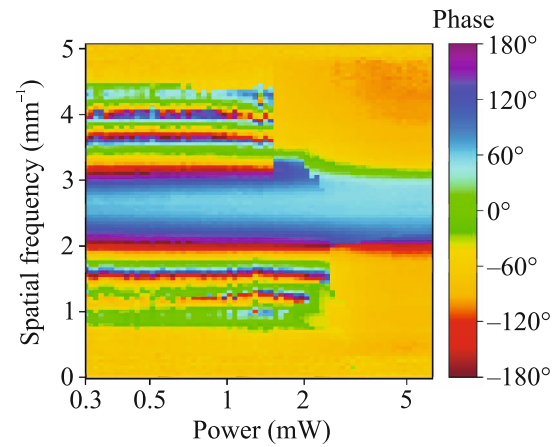

Fig. 2. (Color online) Phase distribution of the magnetization precession signal over the sample under varying the pump power. The formation of spin waves at low pump powers and coherent precession at high pump powers can be seen.

may conclude that the observed coherent state of magnons is beyond the applicability limits of the semiclassical approximation in this case.

The discussion of the results obtained in [37] raises the question of the conditions for the transition from the spin-wave dynamics to the formation of the magnon Bose−Einstein condensate. In this paper, we report the results of the related experiment. We performed these investigations using the same sample as in [37]. The excitation strip was placed at the center of the sample (an ordinate of 2.5 in Figs. 1 and 2). The experiment was carried out at a fixed field strength reduced by 3 Oe from the Larmor resonance field at this frequency. Figure 1 shows the amplitude of deviation of the precessing magnetization in a magnetic disk with a change in the pump power. In the weak-excitation limit, one can see that the magnetization deviates significantly only in the excitation region. Beyond the excitation region, the deviation is about 2° or less (except for a small local region near the excitation strip). With an increase in the pump power to 1.6 mW, the amplitude of the magnetization precession increases in a threshold manner in the region above the excitation region; at a power of 2.5 mW, it also increases below the excitation region. In both regions, the precession angle exceeds 5° in a threshold way. We may conclude that mBEC regions were formed at this power. Note that magnon dissipation processes were significantly weakened (as previously shown for antiferromagnets), which leads to a stepwise increase in the precession amplitude. The precession deviation angle barely changes with an increase in the pump power because the magnon density in the BEC is determined by the frequency difference rather than by the pump power. This effect is another evidence of the mBEC formation.

The most interesting results are shown in Fig. 2, which presents the precession phase distribution upon variation in the pump power. The formation of spin waves at a low pump power can be clearly seen. When the pump power exceeds 1.6 mW, spin waves disappear above the excitation region, and the magnetization precession becomes coherent. In this case, the magnetization deviation angle and, thereby, the magnon density increase to a value above 3°. The same process occurs in the lower part of the sample with an increase in the pump power above 2.5 mW. Thus, one can directly observe the formation of the coherent state of the magnetization precession corresponding to the magnon Bose−Einstein condensate.

Note that the precession phase changes sharply from about 90° in the excitation region to −90° beyond this region. In addition, the phase rotation direction beyond the excitation region becomes asymmetric. This effect requires further investigation.

Thus, we experimentally observed the transition of the magnetization precession beyond the excitation region from the spin wave mode to the coherent precession mode, when the magnon density exceeded the critical value for the formation of the magnon BEC (theoretically predicted at a magnetization deviation angle of 2.5°). A natural condition for the mBEC formation is the establishment of the necessary magnon density along the whole distance from the excitation region to the sample edge. A small difference between the transitions in the upper and lower parts of the sample is likely due to the inhomogeneity of local relaxation processes in it.

To study the spatial coherence of the precession of magnons, we analyzed excited magnons at different pump powers. To this end, we applied the inverse discrete Fourier transform (IDFT) to the signal with respect to the spatial position along the sample (vertical axis, in millimeters). Then, the Fourier transform amplitude was normalized to unity for each pump
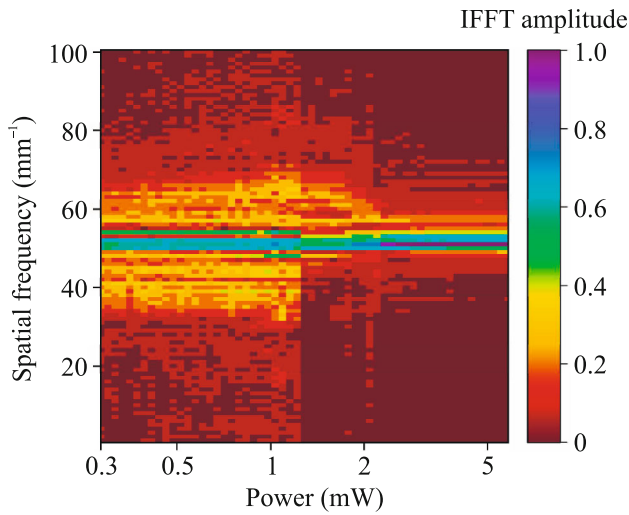
Fig. 3. (Color online) (Pump power, spatial frequency) map of the amplitude of the inverse fast Fourier transform (IFFT).

Fig. 4. (Color online) (Pump power, spatial frequency) map of the amplitude of the inverse fast Fourier transform (IFFT) for the upper part of the sample with the magnon excitation region excluded. The spatial coherence of magnons at a sufficiently high pump power can be clearly seen.

power. The inverse discrete Fourier transform was performed using the radix-2 Cooley−Tukey algorithm, for which one can write a centrosymmetric relation for the reconstruction of the right half from $N/2$ to N of the inverse fast Fourier transform (IFFT) from its left half from 1 to $N/2$:

$$f_{(N-i)} = f_i^*, \quad i = 1, 2, \ldots, \lfloor N/2 \rfloor, \tag{2}$$

where f is the spatial frequency in inverse millimeters and $\lfloor N/2 \rfloor$ denotes the floor function, i.e., integer part of $N/2$. The normalized Fourier transform amplitudes obtained depending on the spatial frequency were combined into a single matrix, and the (spatial frequency, power) maps of the normalized amplitude of the inverse fast Fourier transform were plotted. Figure 3 shows the results of the inverse fast Fourier transform for the entire sample from 0 to 4.5 mm, depending on the pump power. One can see a significant narrowing of the line at 1.25 and 2 mW, which is due to the formation of the Bose−Einstein condensate in the upper and lower parts of the sample, respectively. However, the analysis region contains not only the BEC regions but also the excitation region, which naturally has different characteristics because the continuous excitation of magnons occurs in this region with a phase determined by the pump field. To investigate the spectrum of the Bose−Einstein condensate more thoroughly, we performed a similar analysis for only the upper part of the sample from 3.2 to 4.5 mm, disregarding the excitation region. The result is shown in Fig. 4. The central line of the spectrum became much narrower, which indicates the formation of a simply connected region of magnon Bose−Einstein condensation. Note also that, in view of the Fourier transform properties, the linewidth is determined by the sample si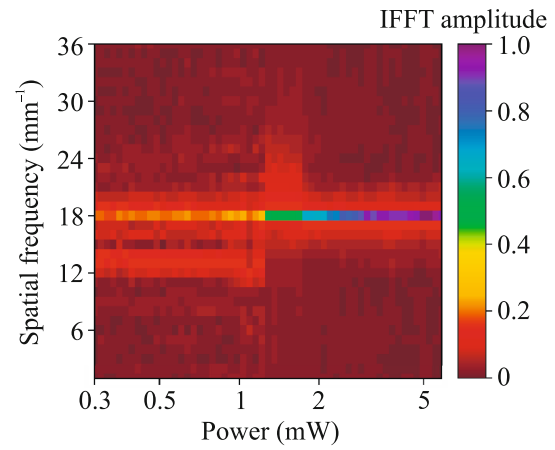ze. If the sample were infinite and the pump power were sufficient for magnon condensation, the formed spectral line would be described by a delta function.

To summarize, we have experimentally observed the transition from spin-wave dynamics, described by the Landau−Lifshitz−Hilbert equations, to the formation of the magnon Bose−Einstein condensate. In this study, the transition of magnons from the gas state to the state of the magnon Bose−Einstein condensate for magnons with $k = 0$ in a perpendicularly magnetized YIG film has been directly detected. The critical magnon density at the transition is in agreement with the previously predicted value corresponding to the angles of dynamic deviation of the precessing magnetization above 3°. This study has shown that the properties of the formed magnon Bose−Einstein condensate are very close to those of the atomic Bose−Einstein condensate. We may also conclude that the magnon Bose−Einstein condensate due to the acoustic excitation of magnons was observed in [39].

FUNDING

CONFLICT OF INTEREST

The authors of this work declare that they have no conflicts of interest.

OPEN ACCESS

REFERENCES

1. M. H. Anderson, J. R. Ensher, M. R. Matthews, C. E. Wieman, and E. A. Cornell, Science (Washington, DC, U. S.) **269**, 198 (1995).

2. K. B. Davis, M.-O. Mewes, M. R. Andrews, M. J. van Druten, D. S. Durfee, D. M. Kurn, and W. Ketterle, Phys. Rev. Lett. **75**, 3969 (1995).

3. J. Klaers, J. Schmitt, F. Vewinger, and M. Weitz, Nature (London, U.K.) **468**, 545 (2010).

4. J. Schmitt, T. Damm, F. Vewinger, and M. Weitz, Appl. Phys. B **105**, 17 (2011).

5. J. L. Figueiredo, J. T. Mendonça, and H. Terças, Phys. Rev. E **108**, L013201 (2023).

6. G. E. Volovik, J. Low Temp. Phys. **153**, 266 (2008).

7. D. M. Stamper-Kurn, A. P. Chikkatur, A. Görlitz, S. Inouye, S. Gupta, D. E. Pritchard, and W. Ketterle, Phys. Rev. Lett. **83**, 2876 (1999).

8. L. A. Melnikovsky, Phys. Rev. B **84**, 024525 (2011).

9. L. V. Butov, A. L. Ivanov, A. Imamoglu, P. B. Littlewood, A. A. Shashkin, V. T. Dolgopolov, K. L. Campman, and A. C. Gossard, Phys. Rev. Lett. **86**, 5608 (2001).

10. B. Deveaud-Pledran, J. Opt. Soc. Am. B **29**, A138 (2012).

11. J. Kasprzak, M. Richard, S. Kundermann, A. Baas, P. Jeambrun, J. M. J. Keeling, F. M. Marchetti, M. H. Szymaska, R. Andre, J. L. Staehli, V. Savona, P. B. Littlewood, B. Deveaud, and L. S. Dang, Nature (London, U.K.) **443**, 409 (2006).

12. A. S. Borovik-Romanov, Yu. M. Bun'kov, V. V. Dmitriev, and Yu. M. Mukharskii, JETP Lett. **40**, 1033 (1984).

13. I. A. Fomin, JETP Lett. **40**, 1037 (1984).

14. Yu. M. Bunkov, J. Phys.: Condens. Matter **21**, 164201 (2009).

15. Yu. M. Bunkov and G. E. Volovik, J. Phys.: Condens. Matter **22**, 164210 (2010).

16. Yu. M. Bunkov, J. Low Temp. Phys. **185**, 399 (2016).

17. A. S. Borovik-Romanov, Yu. M. Bunkov, V. V. Dmitriev, Yu. M. Mukharskiy and D. A. Sergatskov, Phys. Rev. Lett. **62**, 1631 (1989).

18. Yu. M. Bunkov and G. E. Volovik, in *Novel Superfluids, Vol. 1,* Ed. by K. H. Bennemann and J. B. Ketterson, Vol. 156 of *Int. Ser. Monographs on Physics* (Oxford Univ., New York, 2013), p. 253.

19. A. A. Serga, C. W. Sandweg, V. I. Vasyuchka, M. B. Jungfleisch, B. Hillebrands, A. Kreisel, P. Kopietz, and M. P. Kostylev, Phys. Rev. B **86**, 134403 (2012).

20. Yu. M. Bunkov, E. M. Alakshin, R. R. Gazizulin, A. V. Klochkov, V. V. Kuzmin, V. S. L'vov, and M. S. Tagirov, Phys. Rev. Lett. **108**, 177002 (2012).

21. L. V. Abdurakhimov, M. A. Borich, Yu. M. Bunkov, R. R. Gazizulin, D. Konstantinov, M. I. Kurkin, and A. P. Tankeyev, Phys. Rev. B **97**, 024425 (2018).

22. Yu. M. Bunkov, A. V. Klochkov, T. R. Safin, K. R. Safiulin, and M. S. Tagirov, JETP Lett. **109**, 40 (2019).

23. Yu. M. Bunkov, P. M. Vetoshko, A. N. Kuzmichev, G. V. Mamin, S. B. Orlinskii, T. R. Safin, V. I. Belotelov, and M. S. Tagirov, JETP Lett. **111**, 62 (2020).

24. P. M. Vetoshko, G. A. Knyazev, A. N. Kuzmichev, A. A. Kholin, V. I. Belotelov, and Yu. M. Bunkov, JETP Lett. **112**, 299 (2020).

25. Yu. M. Bunkov and V. L. Safonov, J. Magn. Magn. Mater. **452**, 30 (2018).

26. Yu. M. Bunkov and G. E. Volovik, J. Phys.: Condens. Matter **22**, 164210 (2010).

27. Yu. M. Bunkov and G. E. Volovik, J. Low Temp. Phys. **150**, 135 (2008).

28. R. P. Feynman, R. B. Leighton, and M. Sands, *The Feynman Lectures on Physics* (Basic Books, New York, 2011).

29. A. C. Borovik-Romanov, Yu. M. Bun'kov, V. V. Dmitriev, Yu. M. Mukharskii, E. V. Podd'yakova, and O. D. Timofeevskaya, Sov. Phys. JETP **69**, 542 (1989).

30. S. O. Demokritov, JETP Lett. **115**, 691 (2022).

31. Yu. M. Bunkov, JETP Lett. **115**, 694 (2022).

32. Yu. M. Bunkov, Appl. Mag. Res. **51**, 1711 (2020).

33. A. C. Borovik-Romanov and N. M. Kreines, Phys. Rep. **81**, 353 (1982).

34. Yu. M. Bunkov, P. M. Vetoshko, T. R. Safin, and M. S. Tagirov, JETP Lett. **117**, 313 (2023).

35. P. E. Petrov, P. O. Kapralov, G. A. Knyazev, A. N. Kuzmichev, P. M. Vetoshko, Yu. M. Bunkov, and V. I. Belotelov, Opt. Express **30**, 1737 (2022).

36. P. E. Petrov, P. O. Kapralov, G. A. Knyazev, A. N. Kuzmichev, P. M. Vetoshko, Yu. M. Bunkov, and V. I. Belotelov, Opt. Express **31**, 8335 (2023).

37. G. A. Knyazev, A. N. Kuzmichev, P. E. Petrov, I. V. Savochkin, P. M. Vetoshko, V. I. Belotelov, and Yu. M. Bunkov, preprint (2023). https://doi.org/10.1364/opticaopen.24591147

38. A. Vansteenkiste, J. Leliaert, M. Dvornik, M. Helsen, F. Garcia-Sanchez, and B. van Waeyenberge, AIP Adv. **4**, 107133 (2014).

39. G. A. Knyazev, A. N. Kuzmichev, P. E. Petrov, P. M. Vetoshko, V. I. Belotelov, and Yu. M. Bunkov, JETP Lett. **118**, 603 (2023).

Translated by A. Sin'kov